AGU PUBLICATIONS

JGR

Journal of Geophysical Research: Space Physics

RESEARCH ARTICLE

10.1002/2015JA021393

Key Points:

- Appearance of SED/TOI structures in the geomagnetic storm late recovery phase
- UT dependency of the SED/TOI strength
- TEC enhancements mainly occurred in the topside ionosphere

Correspondence to:
J. Liu,
jingliu@ucar.edu

Citation:
Liu, J., T. Nakamura, L. Liu, W. Wang, N. Balan, T. Nishiyama, M. R. Hairston, and E. G. Thomas (2015), Formation of polar ionospheric tongue of ionization during minor geomagnetic disturbed conditions, *J. Geophys. Res. Space Physics*, *120*, 6860–6873, doi:10.1002/2015JA021393.

Received 29 APR 2015
Accepted 18 JUL 2015
Accepted article online 25 JUL 2015
Published online 13 AUG 2015

Formation of polar ionospheric tongue of ionization during minor geomagnetic disturbed conditions

Jing Liu[1,2], Takuji Nakamura[3], Libo Liu[1], Wenbin Wang[2], Nanan Balan[3], Takanori Nishiyama[3], Marc R. Hairston[4], and E. G. Thomas[5]

[1]Key Laboratory of Earth and Planetary Physics, Institute of Geology and Geophysics, Chinese Academy of Sciences, Beijing, China, [2]High Altitude Observatory, National Center for Atmospheric Research, Boulder, Colorado, USA, [3]National Institute of Polar Research, Tokyo, Japan, [4]Center for Space Sciences, University of Texas at Dallas, Richardson, Texas, USA, [5]Bradley Department of Electrical and Computer Engineering, Virginia Tech, Blacksburg, Virginia, USA

Abstract Previous investigations of ionospheric storm-enhanced density (SED) and tongue of ionization (TOI) focused mostly on the behavior of TOI during intense geomagnetic storms. Little attention has been paid to the spatial and temporal variations of TOI during weak to moderate geomagnetic disturbed conditions. In this paper we investigate the source and development of TOI during a moderate geomagnetic storm on 14 October 2012. Multi-instrumental observations including GPS total electron content (TEC), Defense Meteorological Satellite Program (DMSP) in situ measured total ion concentration and ion drift velocity, SuperDARN measured polar ion convection patterns, and electron density profiles from the Poker Flat Incoherent Scatter Radar (PFISR) have been utilized in the current analysis. GPS TEC maps show salient TOI structures persisting for about 5 h over high latitudes of North America on 14 October 2012 in the later recovery phase of the storm when the magnitudes of IMF By and Bz were less than 5 nT. The PFISR electron density profiles indicate that the extra ionization for TEC enhancements mainly occurred in the topside ionosphere with no obvious changes in the bottomside ionosphere and vertical plasma drifts. Additionally, there were no signatures of penetration electric fields in the equatorial electrojet data and upward ion drifts at high latitudes. At the same time, strong subauroral polarization streams with ion drift speeds exceeding 2.5 km/s carried sunward fluxes and migrated toward lower latitudes for about 5° based on the DMSP cross-track drift measurements. Based on those measurements, we postulate that the combined effects of initial build-up of ionization at midlatitudes through daytime production of ionization and equatorward (or less poleward than normal daytime) neutral wind reducing downward diffusion along the inclined filed lines, and an expanded polar ion convection pattern and its associated horizontal plasma transport are important in the formation of the TOI.

1. Introduction

In the early phase of geomagnetic storms, a large increase in ionosphere F2 region electron density appears frequently at middle latitudes in the afternoon to dusk sector. This positive ionospheric storm effect was initially termed as the "dusk effect" [e.g., *Papagiannis et al.*, 1971; *Mendillo et al.*, 1972; *Buonsanto*, 1995a, 1995b]. Later, this phenomenon was renamed as storm-enhanced density (SED), which is typically featured by high electron densities, elevated *F* region peak, and low electron temperatures near sunset at middle latitudes [*Foster*, 1993]. It is regarded as the ionospheric signatures of plasmaspheric tails [*Foster et al.*, 2002; *Yizengaw et al.*, 2008]. Such effects have a favored longitude for occurrence over the North American continent where both the sunlit ionization and upward plasma drifts are large because its location is far from the geographic pole but close to the magnetic pole [*Sojka et al.*, 2012]. The ionosphere at the locations far from the geographic pole has stronger solar ionization because of the smaller solar zenith angle, while the locations close to the magnetic pole have greater upward ion drifts due to electric fields.

Several mechanisms are proposed for the formation of the SED, including electrodynamics, neutral dynamics, and external ionization caused by energetic particle precipitations. *Foster* [1993] proposed that the expanded high-latitude convection electric field continuously encounters the solar-produced plasma at its equatorward edge and generates a latitudinally narrow region of SED in front of the expanded convection pattern. *Deng and Ridley* [2006] suggested that local solar-produced plasma that is transported upward and poleward by the convection electric field might be the primary source of SED. This idea is also supported by the work of *Heelis et al.* [2009].

It is also suggested that equatorial *F* region plasma that is carried to higher altitudes by the large storm time E × B drift diffuses to higher latitudes along the magnetic field lines and thus contribute to the SED generation [e.g., *Kelley et al.*, 2004; *Tsurutani et al.*, 2004]. Based on the coupled magnetosphere ionosphere thermosphere model outputs in the initial phase of three intense storms, *Wang et al.* [2010] reinforced the importance of electric fields in producing the positive ionospheric storm effects at midlatitudes. *Lu et al.* [2012] performed a comprehensive modeling study of the role of electric fields and disturbance meridional winds in lifting ionospheric plasmas and revealed the importance of disturbance meridional winds to the positive ionospheric storm effects at middle latitudes in the 9 November 2004 storm. The physical mechanisms involved in the cause of the positive storm effects have been examined by a number of researches [e.g., *Balan et al.*, 2010]. A combined effect of equatorward neutral wind and westward E × B drift is also proposed to produce the strong positive ionospheric storm phase [*Anderson*, 1976].

Utilizing multi-instrument observations including GPS total electron content (TEC) and Poker Flat Incoherent Scatter Radar (PFISR), *Zou et al.* [2013] divided a SED event into two parts during the 24–25 October 2011 intense geomagnetic storm and discussed the different dominant mechanisms of these two parts. The first part is caused by the upward vertical motions because of the northward component of the expanded polar convection pattern, while the second part is the combined effects of upward flows, horizontal advection, energetic particle precipitation, and thermospheric winds. It is clear from the above suggested mechanisms that there is no consensus yet regarding the causes of SED.

The SED sometimes can be transported poleward along convection trajectories from the source region at middle latitudes to the polar cap region and form a “tongue”-like structure in the noon-midnight direction. When it enters the polar cap region, it may become a large-scale (~1000 km) tongue of ionization (TOI). Convection electric fields play a decisive role in generating a TOI from midlatitude SED [e.g., *Thomas et al.*, 2013]. If the convection electric fields previously bringing the plasma from midlatitudes into the polar cap become weakened or no longer exist, the SED stagnates as a fossil feature, and no TOI is produced. There could be a TOI independent of any storm-enhanced densities, so in that case the SED would merge with an already existing TOI. Occurrence of TOI feature has a preferable UT and seasonal dependence [*Sojka et al.*, 1994] that may be independent of storm condition.

The electron densities of SED/TOI can be 2–10 times larger than the background values. The steep density gradients at the edges of a TOI can cause plasma instabilities and irregularities of different scales and seed small-scale plasma turbulence, producing disturbances to trans-ionosphere communication and affecting satellite telecommunication and navigation systems. Thus, the SED/TOI has received much attention in both the space research and application communities. Extensive investigations based on observations and numerical simulations have been performed on the evolution of TOI during intense geomagnetic storms driven by interplanetary coronal mass ejection (ICME) [e.g., *Foster et al.*, 2005; *Hosokawa et al.*, 2010; *David et al.*, 2011; *Thomas et al.*, 2013; *Zou et al.*, 2013]. Using multi-radar data covering subauroral latitudes, cusp, and polar cap regions, *Foster et al.* [2005] examined the generation and characteristics of TOI during the 20 November 2003 superstorm event and indicated that polar cap TOI was formed as a result of the transport of the midlatitude SED due to subauroral polarization streams (SAPS), which are strong westward/sunward flows in the afternoon and premidnight sectors caused by poleward electric fields in the subauroral latitudes. *Hosokawa et al.* [2010] analyzed a TOI event in the main phase of the 14–16 December 2006 strong magnetic storm and concluded that both the expanded high-latitude plasma convection and midlatitude enhanced plasma density were necessary for the generation of TOI. *Pokhotelov et al.* [2009] reported that corotating interaction region (CIR)-driven storm during 1400–1700 UT on October 2002 produced dramatic enhancements in the polar ionosphere and generated a TOI. The TEC anomalies in the polar ionosphere during this CIR-driven storm resembled the behaviors of those during ICME-driven storms in morphology and time scales. Equatorward neutral winds of low to high speed (depending on the amount of energy input) that flow from high to low latitudes during disturbed periods can stop (or reduce) the accumulated plasma from diffusing downward along the field lines to low altitudes of heavy chemical loss and thus may also contribute to the formation and maintenance of TOI [e.g., *Balan et al.*, 2013].

Previous investigations mostly focus on TOI during major geomagnetic disturbed conditions when the polar plasma convection pattern expands dramatically and daytime positive ionospheric storm effects are likely to occur at middle latitudes [e.g., *Foster et al.*, 2005; *Hosokawa et al.*, 2010]. The behaviors of TOI

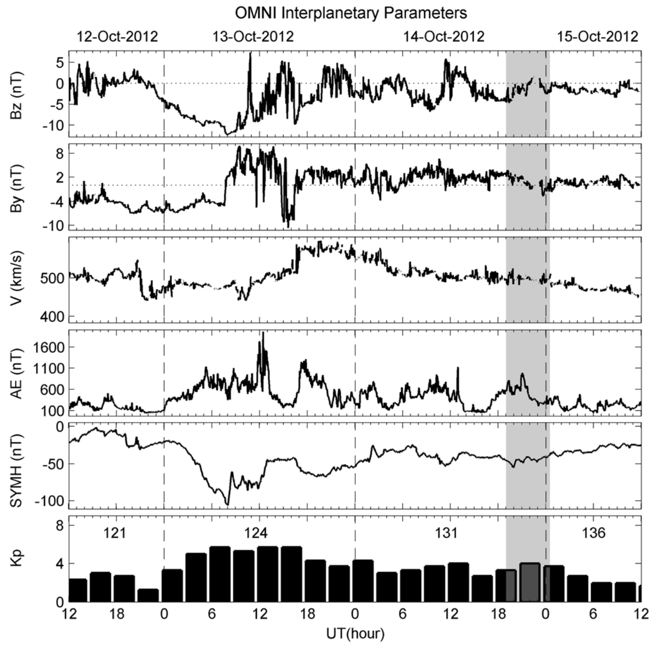

Figure 1. Geomagnetic and solar wind parameters from 12 UT on 12 October to 12 UT on 15 October 2012: (from top) OMNI IMF Bz, By, solar wind velocity, AE index, Sym-H index, and Kp index. The shaded region indicates the interval when the TOI structure formed as identified from GPS TEC maps.

during moderately geomagnetic disturbed conditions, especially in the later recovery phase of storms, however, have not yet been reported. The main objective of this work is to investigate the temporal and spatial variations of TOI during weak geomagnetically disturbed conditions and identify the origin of the TOI. The remaining parts of the paper are organized as follows. Section 2 presents a detailed analysis of the TOI event. The origin of the TOI will be discussed in section 3, and a summary is given in section 4.

2. Event Analysis

Figure 1 displays the variations of interplanetary magnetic field (IMF) Bz and By components in GSM coordinates, solar wind velocity (*V*), the AE index, the SYM-H index, and the Kp index from 12 UT on 12 October to 12 UT on 15 October 2012. The solar wind parameters are provided by the OMNI 2 database (ftp://spdf.gsfc.nasa.gov/pub/data/omni/high_res_omni/). The magnitude of the daily F10.7 index is labeled in the bottom panel. The symmetric component of the ring current (SYM-H) can be viewed as a high temporal resolution Dst index, and the AE index represents the auroral substorm intensity. The shaded region corresponds to the interval of the TOI.

On 12 October, IMF Bz and By fluctuated between −5 nT and 5 nT, the solar wind speed was about 500 km/s, and magnetic activity was weak. IMF Bz turned southward at ~2200 UT on 12 October 2012 and reached a minimum at 0757 UT on 13 October 2012. During this period, IMF By was negative with a magnitude of about 4 nT. The southward IMF Bz triggered the geomagnetic storm main phase at around 0100 UT on 13 October. SYM-H reached a minimum of −106 nT at ~0800 UT on 13 October and then recovered gradually. The AE index increased gradually in the main phase and increased abruptly in the early recovery phase to a maximum value of ~2000 nT at ~1200 UT, and the Kp index reached 6^{-}. A substorm took place in the late recovery phase of the storm at 1635–2315 UT on 14 October, which was characterized by an abrupt increase in the AE index with a maximum value of ~1000 nT. IMF Bz was southward but its magnitude was smaller than 5 nT, while the IMF By component changed gradually from positive to negative values, and the solar wind speed smoothly decreased. During this interval, the substorm produced a salient TOI structure, which is the topic for the current study.

Figure 2 shows the evolution of high-latitude ionospheric TEC and plasma convection in the magnetic local time (MLT)-magnetic latitude (MLAT) coordinates at an hourly cadence. The ionospheric TEC data with a 5 min resolution were obtained from the Madrigal database [*Rideout and Coster*, 2006]. A standard spatiotemporal median filtering technique was used to generate the 2D TEC map. SuperDARN plasma convection streamlines are superposed in each subfigure. The electrostatic potential lines were obtained through spherical harmonic fitting of the line-of-sight velocity observed by SuperDARN radars [*Ruohoniemi and Baker*, 1998; *Shepherd and Ruohoniemi*, 2000]. Following the substorm commencement at ~1635 UT on 14 October (Figure 1), the high-latitude convection pattern at 1900 UT expanded compared to that at 1700 UT as illustrated in Figure 2. At around 1900 UT on 14 October, a TEC plume (enhanced TEC structure) began to emerge in the cusp region over Northern America as a continuation of the high-density plasma at midlatitudes probably formed by daytime production and equatorward (or less poleward than normal) neutral wind. As time progressed, the enhanced TEC structure gradually propagated into the polar cap

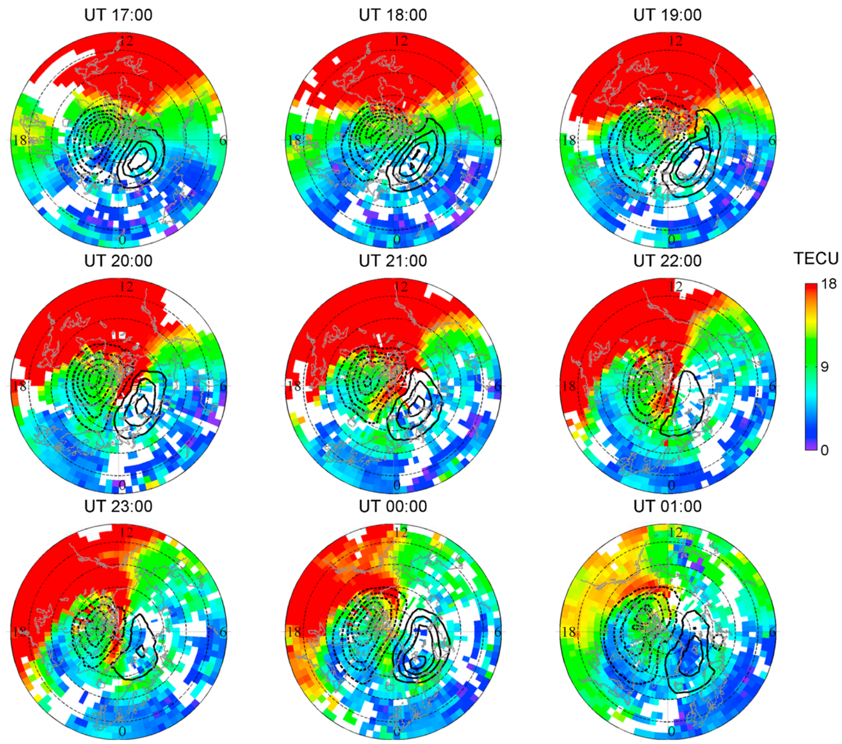

Figure 2. Sequences of GPS TEC maps in the coordinates of MLAT (40–90°) and MLT during 1700 UT on 14 October to 0100 UT on 15 October 2012. Plasma convection patterns observed by SuperDARN are superposed.

toward the midnight sector along the plasma convection streamlines. A complete TOI structure appeared at around 2200 UT on 14 October with the leading edge terminated at the deflection points of the high-latitude convection at 23 MLT. The TOI trailing edge near noon was over the Alaska region where PFISR is installed. The TOI structure was sustained for about 5 h.

Since TEC is the total column density from the bottomside ionosphere to the plasmasphere, it is interesting to investigate how the ionosphere varied at fixed altitudes over the course of the TOI event. Figure 3 depicts the total ion density Ni at around 840 km from in situ measurements by DMSP satellites. The DMSP spacecraft are in near-polar Sun-synchronous orbits at a constant geocentric altitude of ~840 km. Total ion density (Ni) and cross-track ion velocity (Vy) were obtained from the Special Sensor Ion Electron Scintillation (SSIES) instrument on board DMSP F16, F17, and F18. Generally speaking, Ni variations at 840 km resembled those of TEC. The TOI structure did not appear during the interval of 0000–1200 UT on 14 October. Moderately enhanced Ni was observed over the east side of the Arctic Ocean during 1700–1830 UT. The enhancements became more evident in the following 5 h, peaked at around 2000–2130 UT, and gradually shifted to the center of the Arctic Ocean.

In order to investigate the correlation between TOI and midlatitude ionospheric electron density changes, Figure 4 shows the variations of GPS TEC in the Alaska longitudes (90°–100°W) and at 1200–1300 MLT as functions of UT and MLAT. The top panel gives the corresponding IMF By and Bz. The chosen longitude and MLT were where and when the TOI started to emerge. The shaded area in the top panel denotes the duration of the occurrence of TOI. During this period, the magnitudes of IMF Bz and By were small and less than 5 nT. The TEC within the range of 60–70° MLAT at noon on 14 October was larger than that on 12 October by about 15 TECU. In the bottom panel, the extension of TEC enhancements into high latitudes started at about 1800 UT on 14 October.

Now we examine plasma drift variations during this period to study the possible correlation between SAPS and TOI, as suggested by *Foster et al.* [2005]. SAPS refer to strong poleward electric fields in a latitudinally narrow subauroral region that drive strong sunward plasma flows in the dusk to midnight sector. SAPS are associated with the midlatitude electron density trough and region 2 field-aligned currents [*Foster and Burke*, 2002; *Foster et al.*, 2007; *Wang et al.*, 2012, 2008, 2014]. Figures 5b–5f show DMSP F18 in situ total

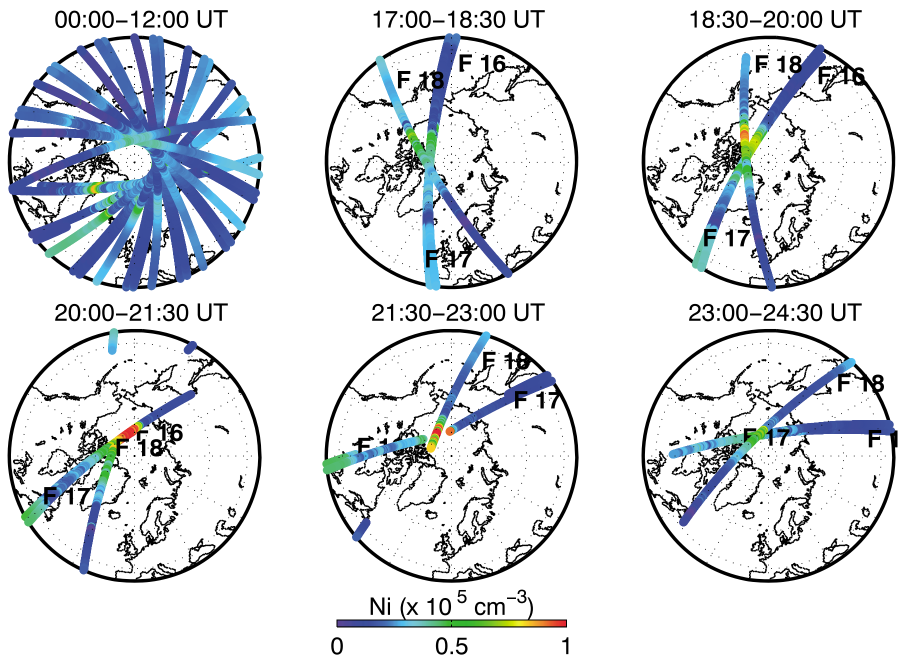

Figure 3. Polar view of in situ DMSP measured total ion density Ni. The interval 0000–1200 UT denotes non-TOI periods. The outer diameter is 40° geographic latitude.

ion density Ni (gray lines) and westward ion drift Vy (colored lines) on the dusk side between 50° and 70° geographic latitude. The ground tracks of the satellite passes are depicted in Figure 5a. The horizontal blue dashed lines in Figures 5b–5f are the equatorward boundaries of auroral precipitations identified from DMSP energy spectrograms. Large cross-track westward drifts associated with SAPS appear in four of the five passes, but caution must be taken with these data because of the details in the drift meter analysis. All five of these plots cover periods when the ion density is below ~2.2×10^4 cm^{-3} except for the portion between 65° and 68° in Figure 5f. Nominally, the drift meter samples each cross-track flow (horizontal and vertical) six times per second, and the six samples are averaged together to give the final 1 s drift value used in the analysis. But when the density drops below the 2.2×10^4 cm^{-3} level, the drift meter switches to a single sample per second mode for each cross-track drift. When the density falls to roughly 1.5 to 2×10^3 cm^{-3}, then the current from the ions entering the drift meter is too small to measure, and we have no data at that time. All four SAPS examined here (Figures 5b and 5d–5f) have a central region that falls below this critical density and have data gaps in the cross-track horizontal (zonal) drift at their center. The question here is at what point do we lose confidence in the validity of the measured cross-track drifts as the density decreases? For data taken when the density is above the critical 2.2×10^4 cm^{-3} level we are generally confident for drift values less than 2800 m/s. For times where the density is between the 2.2×10^4 cm^{-3} and

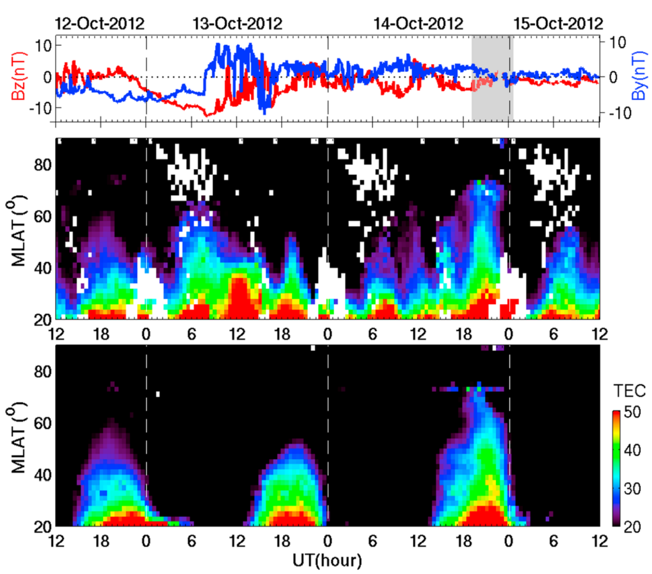

Figure 4. From the top to the bottom are the variations of IMF By and Bz components, and GPS TEC in the Alaska longitude (90°–100° W) and at 12–13 MLT as a function of UT and MLAT.

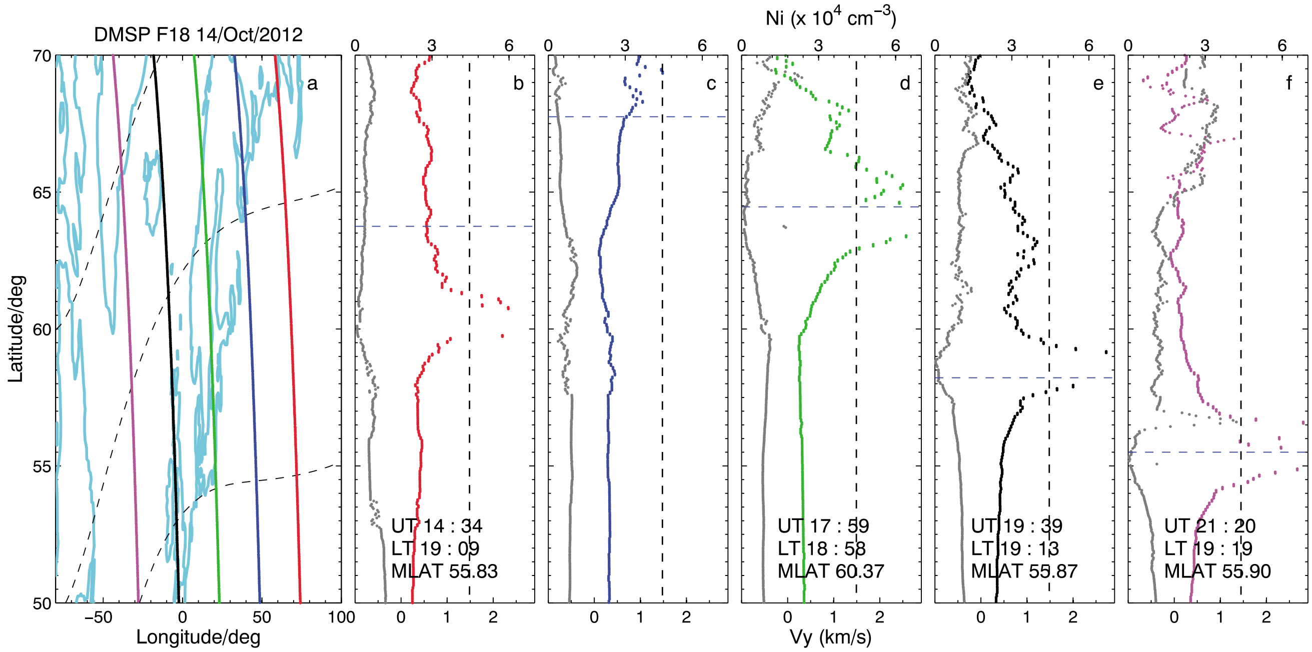

Figure 5. (a) Ground tracks of F18 during the period of 1400–2130 UT on 14 October. The three thin dashed lines represent magnetic latitudes 50°, 60°, and 70°, respectively. (b–f) DMSP F18 measured in situ total ion density Ni (gray lines) and cross-track ion velocity Vy (positive is sunward, colored lines). The universal time, local time, and magnetic latitude of the largest SAPS speed are labeled. The horizontal blue dashed lines give the equatorward boundary of auroral electron precipitation.

2×10^3 cm^{-3} levels, then we are confident about the drift speeds only less than 1500 m/s. Figures 5b–5f have vertical dashed lines denoting this 1500 m/s level. Thus, the data points above the 1500 m/s line indicate that there are large drifts at those times, but we are not certain of their absolute magnitudes. So for these four SAPS events, we do have confidence that the data show that the SAPS are real and they show clear examples of large positive (westward) zonal drifts which define the SAPS, but we cannot say for certain what the absolute flow velocities are in the central regions of each SAPS.

Examining each orbital pass in turn, we note that strong cross-track westward ion drifts at subauroral latitudes are first observed at 1434 UT on 14 October (red, Figure 5b); however, the SAPS disappeared by the time of the next orbit (blue, Figure 5c). In the third orbit (green, Figure 5d), a strong sunward drift reappeared at 1759 UT when the IMF Bz had a magnitude of ~4 nT. The regular auroral convection and SAPS structure are merged together in the third orbit (black, Figure 5e). In the final orbit (magenta, Figure 5f), two peaks are suggested from the zonal drifts. The higher latitude one is the regular convection flow, and the lower latitude one corresponds to the SAPS structure. SAPS migrated toward lower magnetic latitudes for about 5° in the following two orbits (black and magenta, Figures 5e and 5f). Enhanced SAPS electric fields emerged shortly after the first substorm onset at around 1700 UT and continued to dominate the westward plasma convection at subauroral magnetic latitudes 57°–60° N for ~4 h. Additionally, the midlatitude ion trough was present to accompany the SAPS. SAPS have been associated with geomagnetic disturbed conditions and specifically with substorm in the context of substorm-related field-aligned currents and midnight midlatitude electron density trough [*Spiro et al.*, 1979; *Anderson et al.*, 1993; *Karlsson et al.*, 1998]. Premidnight downward region 2 field-aligned currents tend to intensify in the substorm growth and expansion phases, and close with poleward Pedersen currents. The northward electric field is intensified to maintain the current continuity over the low conductivity region of the trough. This drives fast sunward (or westward in the premidnight sector) ion drifts, which lead to increased plasma-neutral collisions and plasma temperature. This, in turn, increases chemical recombination, which further decreases the electron density and ionospheric conductivity in the subauroral trough region, and intensifies the northward electric field and westward ion drifts.

Figure 6 displays DMSP F18 observations of energy spectrograms of electrons and ions in log scale, total plasma density Ni, sunward cross-track velocity Vy, vertical upward velocity Vz, sunward flux Fy, and upward flux Fz on 14 October for orbit f in Figure 5. Flux is the product of velocity and plasma density. As shown in the

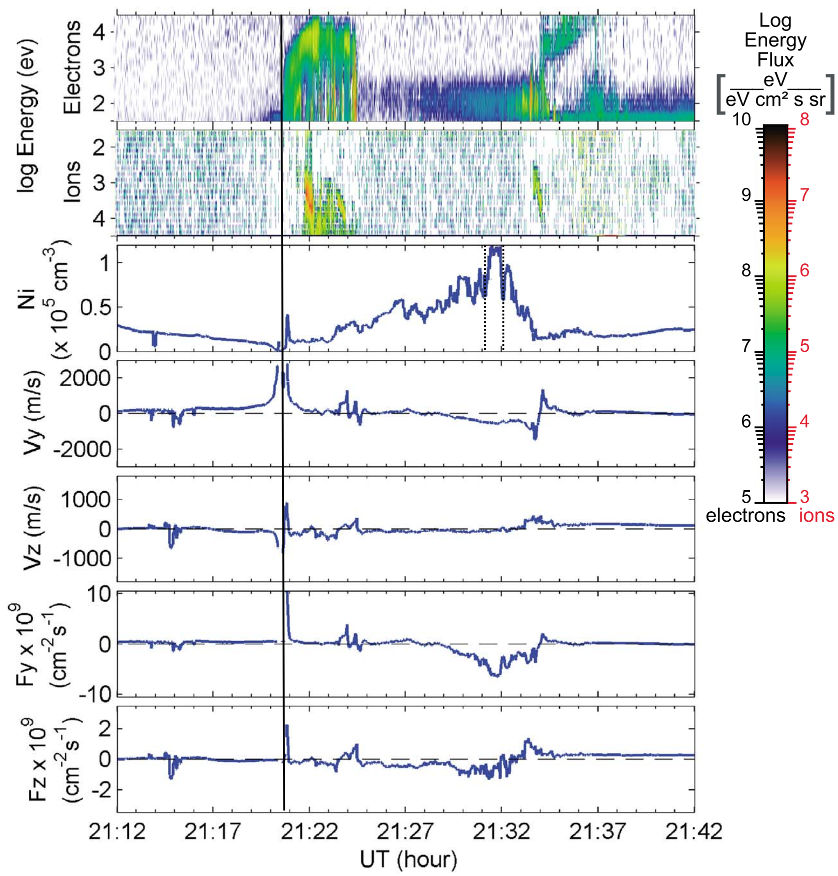

Figure 6. DMSP F18 observations of energy spectrograms of precipitating electrons and ions, total ion density Ni, sunward cross-track velocity Vy, vertical upward velocity Vz, sunward flux Fy, and upward flux Fz. This is the orbit f in Figure 5. The two dotted lines on the Ni graph denote the boundaries of TOI.

top two panels, the equatorward boundaries of electron precipitation were seen at ~2121 UT (indicated by the vertical dark line for the electron boundary) and 2137 UT for the ion boundary. The TOI density enhancement is encountered by the spacecraft in the polar cap region at ~2131 UT. There was a small downward velocity (roughly −100 m/s) and flux which accompanies the TOI structure. Strong sunward flow with a magnitude in excess of 2000 m/s appeared on the duskside lower latitude equatorward boundary.

In order to give a better combined view of different measurements, Figure 7 illustrates the polar view of absolute GPS TEC, plasma convection pattern observed by SuperDARN, cross-track velocity (Vy, blue line), and total plasma density (Ni, dark dotted line) from DMSP in magnetic latitude and magnetic local time coordinates. There are several noticeable features of these DMSP measurements including the SAPS on dusk side, TOI in the polar cap, and a strong Vy flow shear on the morning side. A deep subauroral latitude ion density trough appeared within the region of SAPS. A good agreement between TEC and Ni at 840 km is observed in capturing the TOI structure, in that the Ni at 840 km maximized near the TEC TOI structure. In the morning sector, a very strong flow shear in the Vy component at the convection reversal boundary showed at about 72° magnetic latitude. This was not well captured by the SuperDARN plasma convection pattern, which showed dawnward flow, 5 degree poleward of the DMSP sunward observation.

Figure 8 depicts the temporal variations of the absolute deviations of TEC between the TOI event and a quiet time reference in polar coordinates. The quiet time TEC reference of 12 October is substrated from the TEC values on 14 October for the same UTs. The magnetic latitude circles are 10° apart with the outer circle at 40°. The TEC enhancements at MLT noon spanning from 50° to 70° magnetic latitudes commenced at around 1900 UT. One hour later, the area of enhanced TEC expanded to lower latitudes and the polar cap where the peak enhancement was about 15 TECU. SED was seen in the afternoon sector equatorward and westward of the ionospheric midlatitude latitude trough [e.g., *Foster et al.*, 2005] and also clearly presented at 2000 UT.

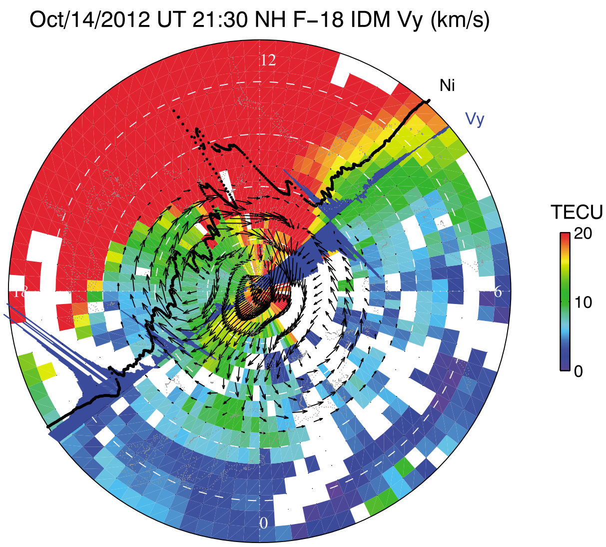

Figure 7. Polar view of absolute TEC, cross-track velocity (Vy, blue line), and total plasma density (Ni, dark dotted line) in the magnetic latitude (40–90°) and magnetic local time coordinate. The *y* axes for Vy and Ni are perpendicular to the orbit. Plasma convection pattern observed by SuperDARN is also superimposed. This satellite progressed from the nighttime sector to the morning sector. This is also the orbit f in Figure 5.

In the following 3 h, the TOI structures propagated further through the magnetic pole and toward the MLT midnight sector. The enhanced daytime TEC in the afternoon was accompanied by a decrease in TEC poleward of the rough between 55° and 70° magnetic latitudes. The TEC trough was barely visible at 1900 UT. Later, this midlatitude trough structure was deepened and widened from 2000 to 2300 UT. Besides this evident TEC depression in the afternoon and nighttime sectors, salient TEC depletion (negative ionospheric phase) also appeared at 40–52° magnetic latitudes in the prenoon sector. TEC negative phase (depleted TEC or electron density) is frequently observed in the morning sector during geomagnetic disturbed conditions, which is mostly related to neutral composition changes [*Liu et al.*, 2010]. Decrease in the O/N2 due to thermospheric heating during geomagnetic storms leads to the negative storm phase [*Prölss*, 1995].

The "+" sign in Figure 8 shows the location of PFISR which was under the base of the TOI at 2300 UT. Figure 9 shows the PFISR electron density, electron temperature, ion temperature profiles. and the upward vertical plasma velocity at around 300 km from 1200 UT on 12 October to 1200 UT on 14 October 2012. The vertical plasma velocity at 300 km is chosen to represent the *F* region plasma drifts because the altitude variation of the vertical plasma velocity in the ionospheric *F* region is small as indicated by its profile (in Figure 10). Compared to 12 October, the electron density profile on 14 October expanded upward in altitude

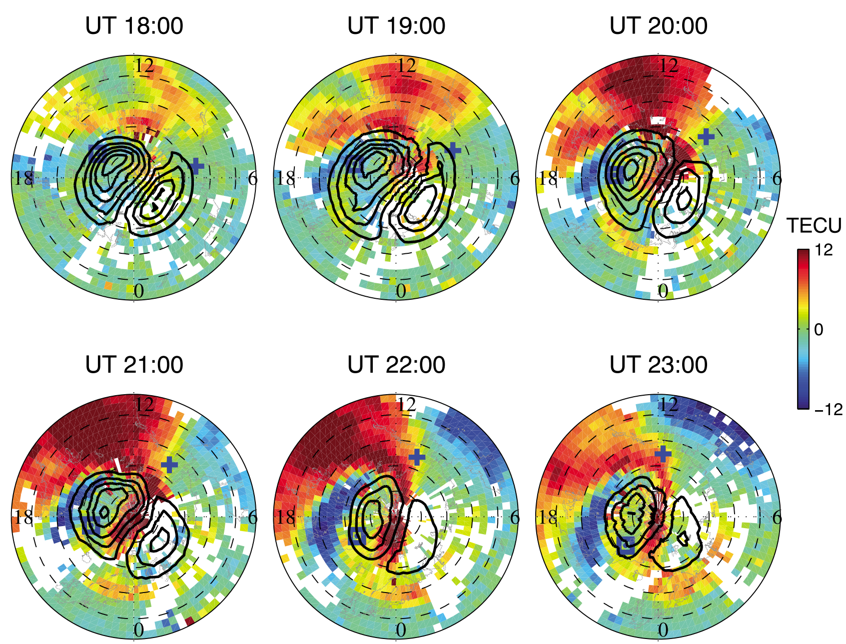

Figure 8. Polar view of relative deviations of storm time TEC in the coordinates of MLAT (40–90°) and MLT on 14 October 2012 with respect to the quiet time reference on 12 October 2012. The "+" and square signs indicate the location of PFISR and Sondrestrom Radar, respectively.

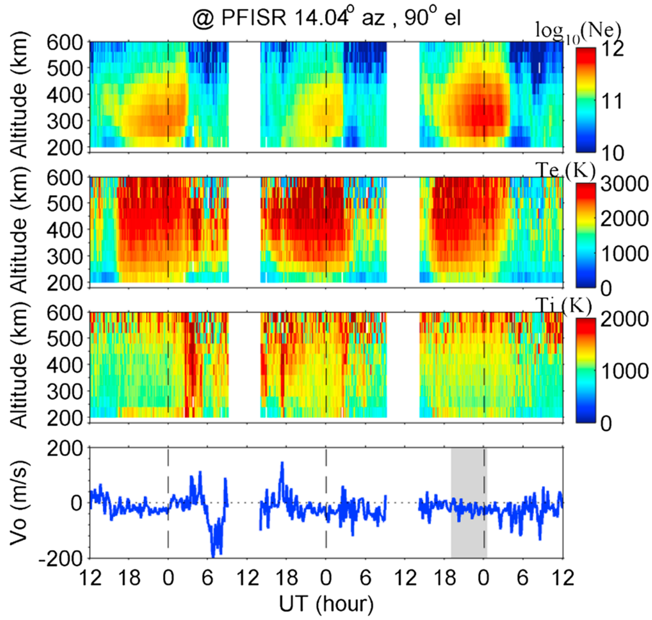

Figure 9. PFISR observed electron density, electron temperature, ion temperature, and upward vertical plasma velocity at around 300 km from 12 UT on 12 October to 12 UT on 15 October 2012.

during 1900–2300 UT, and the electron temperature weakly decreased in the topside ionosphere with no significant changes in the upward plasma drift velocity. To further examine the ionospheric electron density profiles, Figure 10 displays the storm time (red lines) and quiet time (blue dotted lines) profiles of electron density, electron temperature, ion temperature, and vertical plasma velocity over Poker Flat (top panel) and Sondrestrom (bottom panel). The Sondrestrom Radar is located near the west coast of Greenland (geographic 66.99°N and 50.95°W) and makes ionospheric measurements within the dusk polar cap and noontime cusp/cleft region. The electron density enhancements mainly occurred in the topside ionosphere from PFISR (at 2256 UT) with no significant change in hmF2. Both electron and ion temperature were weakly decreased in the topside ionosphere. However, in the polar cap region (Sondrestrom), the electron density profile showed very weak enhancement (at 2205 UT) again with almost no change in hmF2. As shown in Figure 8, Sondrestrom was located in the dusk cell and not in a good position to observe TOI. The weak enhanced density at Sondrestrom may be related to boundary blob as a result of the return plasma flow. The electron and ion temperature displayed very complex behaviors. At both stations, the upward plasma velocity was close to zero and no strong outflow was observed

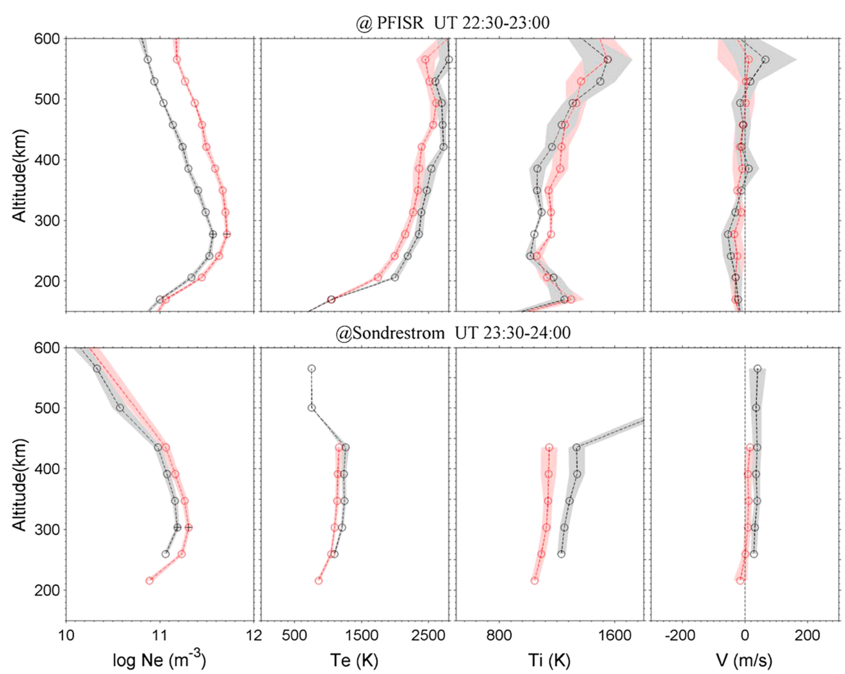

Figure 10. Comparisons between the storm time (red lines) and quiet time (gray lines) values of electron density, electron temperature, ion temperature, and vertical plasma velocity. The dark crosses symbolize the location of hmF2.

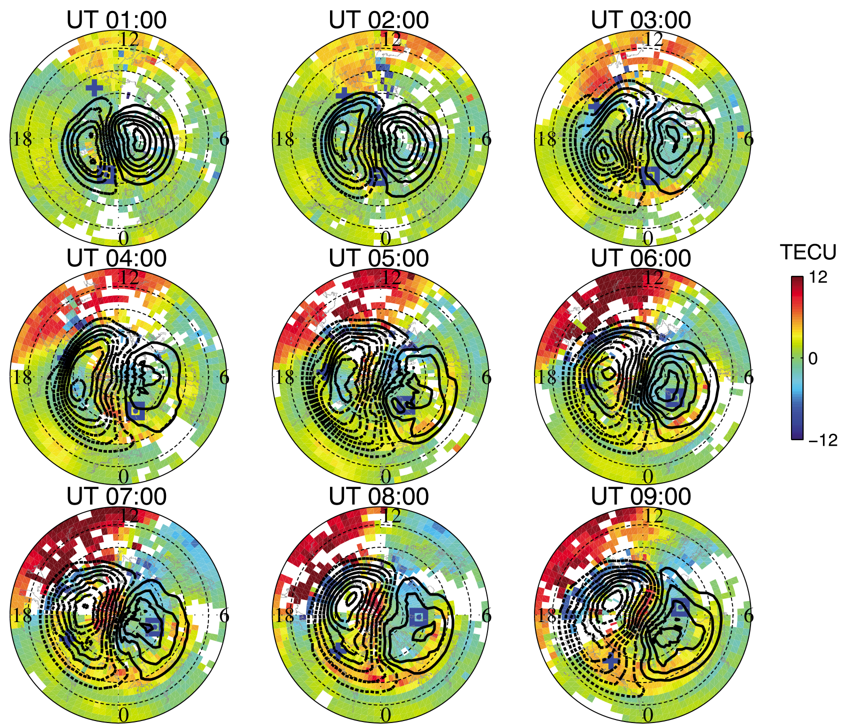

Figure 11. Polar view of relative deviations of storm time TEC in the coordinates of MLAT (40–90°) and MLT on 13 October 2012 with respect to the quiet time reference on 12 October 2012.

whichwere distinctly different from the cases in *Foster et al.* [2005] and *Yuan et al.* [2008]. In their work, very strong upward field-aligned plasma velocities and fluxes associated with SED/TOI were observed in the cusp and polar cap regions.

3. Discussion

3.1. TOI Characteristics During Moderate and Strong Geomagnetic Storms

As far as we are aware, this is the first work that reports the evolution of TOI during the late recovery phase of a geomagnetic storm. It is instructive to investigate the difference between strong and moderate geomagnetic storms and between main and recovery phases in terms of IMF drivers of the storm, TOI structure, and lifetime. In this case, IMF Bz and By were very weak and less than 5 nT in magnitude. We have observed a TOI structure persisting for about 5 h with the appearance of strong SAPS in the context of weak southward IMF Bz. The TOI structure was only confined in the polar cap within 70° magnetic latitude, and its width extended by about 10°. On the contrary, the TOI structure occurring at 1730–2030 UT during the main and early recovery phase of the 20 November 2003 superstorm corresponded to the condition that the IMF Bz was ~−50 nT. It was more extended in both directions with its front approaching 50° magnetic latitude [e.g., *Foster et al.*, 2005]. *Hosokawa et al.* [2010] also showed that a TOI continued for about 4 h during the early recovery phase with a prolonged large southward IMF Bz during the intense geomagnetic storm on 14–16 December 2006. For a weaker geomagnetic storm on 26–27 September 2011, an approximate 1 h long TOI appeared, which was characterized by sustained positive IMF By and a strong southward IMF Bz (less than −20 nT) [*Thomas et al.*, 2013]. As reviewed here, the duration and intensity of TOI do not seem to show a linear dependence on IMF By and Bz conditions.

On the day just before the TOI event in this study, there were no SED/TOI at the same UT, and there was only weak TOI during the main phase of the storm. As shown in Figure 11, the TEC at magnetic latitude 50–70° was also increased in the afternoon sector during 0400–0700 UT. Relative weak TOI structure was observed during 0600–0800 UT when the IMF Bz was strong with the maximum value approaching −15 nT. The reasons leading to this discrepancy could be related to the longitudinal dependence of the TOI occurrence. The 11° displacement between the geographic pole and the magnetic pole in the northern hemisphere creates a UT variation for the convection pattern in geographic coordinates. As a result, the polar convection

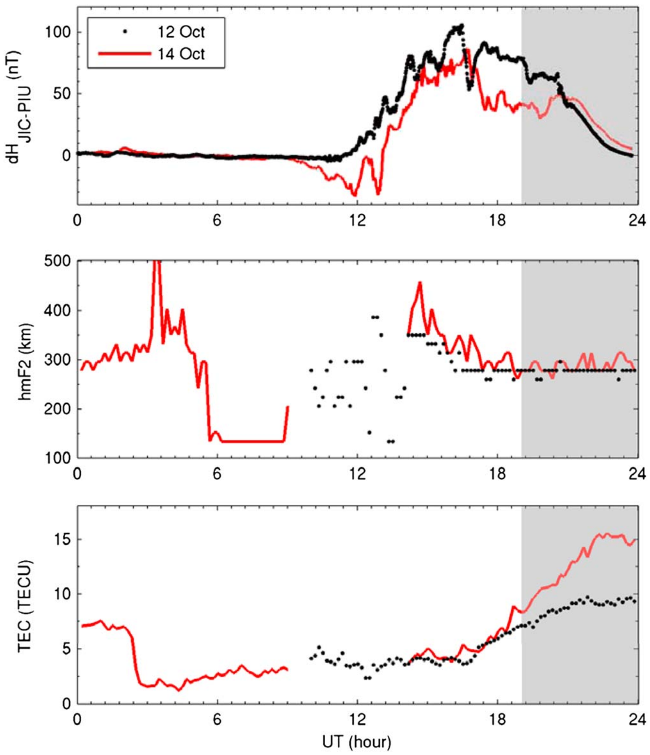

Figure 12. Diurnal variation of $\Delta H_{JIC\text{-}PIU}$, hmF2, and TEC from PFISR. The black dotted line and red line represent the quiet time reference and storm time values, respectively.

pattern in Northern America expands most equatorward in geographic coordinates, which is favorable for bringing high-density plasmas from middle latitudes to high latitudes to generate TOI [*Foster*, 1993; *Sojka et al.*, 2012]. In addition, the negative ionospheric effects at middle and high latitudes during 1800–2400 UT on 13 October as shown in the second panel of Figure 4 did not provide enough plasma material for the formation of TOI even though the polar convection pattern is more equatorward extended compared to it on 14 October.

3.2. Mechanisms of TOI

We used data from different measurements to identify the main mechanisms of this TOI event. Eastward prompt penetration electric field (PPEF) was once thought to be the principle mechanism of SED through two different processes: (1) The E × B drifts due to the PPEF tend to uplift the local ionosphere to higher altitudes where chemical recombination is slower and thus increases electron densities. Using the Utah State University time-dependent ionospheric model (TDIM), *David et al.* [2011] suggested that the density enhancements do not originate from lower latitudes but are due to the uplifting of the F layer by penetration electric fields which are sufficient to account for an increase in TEC. Observations from Millstone Hill ISR and GPS TEC show significant increases of the midlatitude ionospheric *F* region electron densities as a result of daytime eastward penetration electric fields on the 3 April 2004 geomagnetic storm [*Huang et al.*, 2005]. (2) The field perpendicular EB drifts due to eastward electric fields and field-aligned diffusion due to gravity and pressure gradient forces, which in the presence of equatorward (or less poleward than normal daytime) neutral wind can increase the plasma density at low to high-middle latitudes [e.g., *Balan et al.*, 2010]. In some extreme circumstances, TEC at midlatitudes under the sunlit conditions can be dramatically enhanced due to the poleward redistribution of the plasma from low latitudes caused by eastward electric field and equatorward forcing of plasma from high latitudes due to equatorward neutral wind [e.g., *Kelley et al.*, 2004; *Tsurutani et al.*, 2004; *Mannucci et al.*, 2005; *Balan et al.*, 2010].

Penetration electric fields occur as a result of the imbalance between the region 1 field-aligned currents and region 2 field-aligned currents. PPEFs are generally short-lived, are global scale, cause abrupt changes, and are highly regulated by interplanetary solar wind conditions. The global ionosphere responds to PPEF almost instantaneously. The difference between these measured horizontal components of geomagnetic field (H) values at equatorial and off equatorial locations provides a direct measure of the daytime electrojet current and, in turn, the magnitude of the vertical E × B drift velocity in the *F* region ionosphere [*Anderson et al.*, 2002]. H component difference between the dip equator station Jicamarca (12.0°S, 76.8°W, 0.8°N dip latitude) and the off equator station Piura (5.17°S, 80.64°W, 6.8°N dip latitude) (denoted by $\Delta H_{JIC\text{-}PIU}$) has been used as a proxy for electric field disturbance [e.g., *Liu et al.*, 2014]. In the present case (Figure 12), $\Delta H_{JIC\text{-}PIU}$ during 1800–2400 UT on 14 December was weaker than that on 12 December and changed smoothly. Thus, PPEF was unlikely the source for the observed increase in TEC and TOI. In other words, there is a lack of connection between TOI and the lower latitude plasma source. Thus, we can exclude the effects of penetration electric field and the resultant latitudinal transportation due to the effects of PPEF [e.g., *Tsurutani et al.*, 2004; *Mannucci et al.*, 2005].

Latitudinally expanded high-latitude ion convection pattern that introduces eastward and poleward electric fields at subauroral latitudes during geomagnetic storms has also been considered as a potential source of SED and TOI [e.g., *Heelis et al.*, 2009]. The eastward electric field in the presence of inclined magnetic field lines at midlatitudes results in ionospheric elevation on the dayside [e.g., *Deng et al.*, 2006]. The poleward electric field in the afternoon sector tends to drive westward plasma drifts which are opposite to the direction of the Earth rotation. Consequently, plasmas move more slowly in this local time sector [*Papagiannis et al.*, 1971; *Evans*, 1973; *Heelis et al.*, 2009]. If these eastward and poleward electric fields operate simultaneously under the sunlit conditions, they will produce plasma stagnation and dramatic electron density enhancements in the afternoon sector. Equatorward neutral winds tend to occur at subauroral latitudes, especially during disturbed conditions. There are two effects of equatorward neutral wind: (1) reduce the downward ambipolar diffusion of plasma along the geomagnetic field lines and (2) raise the ionosphere to high altitudes of low chemical loss [e.g., *Balan et al.*, 2010]. Thus, the combined effect of the expanded polar convection pattern (eastward and poleward electric fields) and equatorward neutral winds may be a plausible cause of the dramatic electron density enhancement and TOI. Equatorward neutral winds of weak to moderate speeds at high latitudes do not have any significant effect in lifting the ionosphere to high altitudes [e.g., *Balan et al.*, 2013], which also agrees with insignificant changes in hmF2 (Figures 10 and 12) associated with the TOI.

Evidence for the expanded convection pattern was observed (Figure 6) in the SAPS during 2000–2200 UT on 14 October when the convection pattern migrated toward the lower latitudes by about 5°. The convection reversal boundary (Figure 2) also expanded toward lower latitudes during 1900 UT when compared to the pattern at 1700 UT on 14 October. About 1 h later, the TOI structure started to penetrate into the polar cap region. The time delay between the expansion of polar convection and TOI could be due to the time needed to transport the plasma from middle latitudes to the polar cap region.

It was shown in Figures 9 and 10 that the TEC enhancements observed by PFISR mainly occurred in the topside ionosphere and that vertical plasma drifts were small, indicating the important role of horizontal transport of the plasma from the dusk convection cell where the plasma density is higher. In earlier studies [e.g., *Foster et al.*, 2005; *Zou et al.*, 2013], SED were featured by the greatly elevated hmF2, large F2 region peak density, and low electron and ion temperatures. For example, it was shown that hmF2 in the first part of SED increased by more than 100 km with the appearance of strong upward plasma velocity [*Zou et al.*, 2013]. Simulation results from *Deng et al.* [2006] showed that upward ion drift tended to reduce the electron density below the F2 peak, while both vertical ion lift and horizontal transport increased the electron density above the F2 peak. This also implies the greater importance of horizontal convection in the topside ionosphere than in the bottom side ionosphere because of low ion-neutral collision frequencies at high altitudes. Ion production and loss are important in electron density changes at low altitudes, while both horizontal and vertical transportation have appreciable effects on the electron density distribution at high altitudes [*Sojka et al.*, 1981]. Plasma motion toward the pole at midlatitudes will necessarily involve a lifting of the charged particles due to the inclination of the magnetic field lines and increase plasma densities. Unfortunately, we do not have direct evidence of this uplifting and its effect on the formation of TOI. Because PFISR was not exactly underneath the TOI in this event but close to the boundary of the TOI, the height elevation effects were not noticeable even though the ionosphere might be uplifted in the center of the TOI. High-latitude stations with good data were not placed near TOI.

4. Conclusion

Data from multi-instruments are used to analyze a TOI event in a moderate geomagnetic activity event in this work. The TOI structure occurred during the late recovery phase of the storm and lasted for about 5 h. The large-scale characteristics of the TOI event exhibited both similar and distinct behaviors compared to the events reported during intense geomagnetic storms. The distinct behaviors include a weak expansion of the polar ion convection pattern, which caused the TOI to be limited to higher latitudes than those during intense geomagnetic storms. The electron density enhancements mainly occurred in the topside ionosphere with a small increase in hmF2. In addition, there was no upward flux from TOI features as seen in ISR and DMSP satellite observations. The similarities include the formation of TOI being accompanied by a strong sunward flow in the subauroral and auroral region in the MLT afternoon sector. These results suggest that the horizontal transport of plasma from the dusk convection cell to noon cleft associated with the expanded high-latitude convection pattern is important for the formation of this TOI event. Although it is clear that SED/TOI can have multiple causes, it would be interesting to study them at moderate geomagnetic activities to see if statistically they are similar to this case. A modeling study would also be fruitful [e.g., *David et al.*, 2011].

Acknowledgments
The authors are grateful for the accessible databases used in this work. GPS TEC, PFISR, Sondrestrom ISR, and magnetometer data are obtained by the MIT Haystack Observatory Madrigal database (http://www.openmadrigal.org).We thank the Center for Atmospheric Research, University of Massachusetts Lowell for providing the ionogram database. The authors acknowledge the use of SuperDARN data. SuperDARN is a collection of radars funded by national scientific funding agencies of Australia, Canada, China, France, Japan, South Africa, UK, and the USA. We thank Barbara Emery for her useful discussions before submission. This research was supported by the Chinese Academy of Sciences (KZZD-EW-01-3), the National Key Basic Research Program of China (2012CB825604), National Natural Science Foundation of China (41304128, 41321003, and 41229001), and China Postdoctoral Science Foundation. Jing Liu appreciates the support of International Exchange Program of National Institute of Information and Communications Technology. The work by Hairston was supported by the NSF grant Ags-1259508. The National Center for Atmospheric Research is sponsored by the National Science Foundation.

Michael Liemohn thanks two anonymous reviewers for the assistance in evaluating this manuscript.

References

Anderson, D. N. (1976), Modeling the midlatitude *F*-region ionospheric storm using east–west drift and a meridional wind, *Planet. Space Sci.*, *24*, 69–77.

Anderson, D., A. Anghel, K. Yumoto, M. Ishitsuka, and E. Kudeki (2002), Estimating daytime vertical $E \times B$ drift velocities in the equatorial *F*-region using ground-based magnetometer observations, *Geophys. Res. Lett.*, *29*(12), 1596, doi:10.1029/2001GL014562.

Anderson, P. C., W. B. Hanson, R. A. Heelis, J. D. Craven, D. N. Baker, and L. A. Frank (1993), A proposed production model of rapid subauroral ion drifts and their relationship to substorm evolution, *J. Geophys. Res.*, *98*(A4), 6069–6078, doi:10.1029/92JA01975.

Balan, N., K. Shiokawa, Y. Otsuka, T. Kikuchi, D. Vijaya Lekshmi, S. Kawamura, M. Yamamoto and G. J. Bailey (2010), A physical mechanism of positive ionospheric storms at low and mid latitudes through observations and modeling, *J. Geophys. Res.*, *115*, A02304, doi: 10.1029/2009JA014515.

Balan, N., Y. Otsuka, M. Nishioka, J. Y. Liu, and G. Bailey (2013), Physical mechanisms of the ionospheric storms at equatorial and higher latitudes during MP and RP of geomagnetic storms, *J. Geophys. Res. Space Physics*, *118*, 2660–2669, doi:10.1002/jgra.50275.

Buonsanto, M. J. (1995a), Millstone Hill incoherent scatter *F* region observations during the disturbances of June 1991, *J. Geophys. Res.*, *100*, 5743–5755, doi:10.1029/94JA03316.

Buonsanto, M. J. (1995b), A case study of the ionospheric storm dusk effect, *J. Geophys. Res.*, *100*, 23,857–23,869, doi:10.1029/95JA02697.

David, M., J. J. Sojka, R. W. Schunk, M. W. Liemohn, and A. J. Coster (2011), Dayside midlatitude ionospheric response to storm time electric fields: A case study for 7 September 2002, *J. Geophys. Res.*, *116*, A12302, doi:10.1029/2011JA016988.

Deng, Y., and A. J. Ridley (2006), Role of vertical ion convection in the high-latitude ionospheric plasma distribution, *J. Geophys. Res.*, *111*, A09314, doi:10.1029/2006JA011637.

Evans, J. V. (1973), The causes of storm-time increases of the F-layer at mid-latitudes, *J. Atmos. Terr. Phys.*, *35*, 593–616.

Foster, J. C. (1993), Storm-time plasma transport at middle and high latitudes, *J. Geophys. Res.*, *98*, 1675–1689, doi:10.1029/92JA02032.

Foster, J. C., and W. J. Burke (2002), SAPS: A new characterization for sub-auroral electric fields, *Eos AGU Trans.*, *83*, 393–394.

Foster, J. C., P. J. Erickson, A. J. Coster, J. Goldstein, and F. J. Rich (2002), Ionospheric signatures of plasmaspheric tails, *Geophys. Res. Lett.*, *29*(13), 1623, doi:10.1029/2002GL015067.

Foster, J. C., A. J. Coster, P. J. Erickson, J. M. Holt, F. D. Lind, W. Rideout, M. McCready, A. van Eyken, R. J. Barnes, R. A. Greenwald and F. J. Rich (2005), Multiradar observations of the polar tongue of ionization, *J. Geophys. Res.*, *110*, A09S31, doi:10.1029/2004JA010928.

Foster, J., W. Rideout, B. Sandel, W. Forrester, and F. Rich (2007), On the relationship of SAPS to storm-enhanced density, *J. Atmos. Sol. Terr. Phys.*, *69*, 303–313, doi:10.1016/j.jastp.2006.07.021.

Heelis, R. A., J. J. Sojka, M. David, and R. W. Schunk (2009), Storm time density enhancements in the middle-latitude dayside ionosphere, *J. Geophys. Res.*, *114*, A03315, doi:10.1029/2008JA013690.

Hosokawa, K., T. Tsugawa, K. Shiokawa, Y. Otsuka, N. Nishitani, T. Ogawa, and M. R. Hairston (2010), Dynamic temporal evolution of polar cap tongue of ionization during magnetic storm, *J. Geophys. Res.*, *115*, A12333, doi:10.1029/2010JA015848.

Huang, C.-S., J. C. Foster, L. P. Goncharenko, P. J. Erickson, W. Rideout, and A. J. Coster (2005), A strong positive phase of ionospheric storms observed by the Millstone Hill incoherent scatter radar and global GPS network, *J. Geophys. Res.*, *110*, A06303, doi:10.1029/2004JA010865.

Karlsson, T., G. T. Marklund, L. G. Blomberg, and A. Malkki (1998), Subauroral electric fields observed by the Freja satellite: A statistical study, *J. Geophys. Res.*, *103*, 4327–4342, doi:10.1029/97JA00333.

Kelley, M. C., M. N. Vlasov, J. C. Foster, and A. J. Coster (2004), A quantitative explanation for the phenomenon known as storm-enhanced density, *Geophys. Res. Lett.*, *31*, L19809, doi:10.1029/2004GL020875.

Liu, J., B. Zhao, and L. Liu (2010), Time delay and duration of ionospheric total electron content responses to geomagnetic disturbances, *Ann. Geophys.*, *28*, 795–805, doi:10.5194/angeo-28-795-2010.

Liu, J., L. Liu, T. Nakamura, B. Zhao, B. Ning, and A. Yoshikawa (2014), A case study of ionospheric storm effects during long-lasting southward IMF Bz-driven geomagnetic storm, *J. Geophys. Res. Space Physics*, *119*, 7716–7731, doi:10.1002/2014JA020273.

Lu, G., L. Goncharenko, M. J. Nicolls, A. Maute, A. Coster, and L. J. Paxton (2012), Ionospheric and thermospheric variations associated with prompt penetration electric fields, *J. Geophys. Res.*, *117*, A08312, doi:10.1029/2012JA017769.

Mannucci, A. J., B. T. Tsurutani, B. A. Iijima, A. Komjathy, A. Saito, W. D. Gonzalez, F. L. Guarnieri, J. U. Kozyra, and R. Skoug (2005), Dayside global ionospheric response to the major interplanetary events of October 29–30, 2003 "Halloween Storms", *Geophys. Res. Lett.*, *32*, L12S02, doi:10.1029/2004GL021467.

Mendillo, M., M. D. Papagiannis, and J. A. Klobuchar (1972), Average behavior of the midlatitude *F*-region parameters N_T, N_{max} and τ during geomagnetic storms, *J. Geophys. Res.*, *77*, 4891–4895, doi:10.1029/JA077i025p04891.

Papagiannis, M. D., M. Mendillo, and J. A. Klobuchar (1971), Simultaneous storm-time increases of the ionospheric total electron content and the geomagnetic field in the dusk sector, *Planet. Space Sci.*, *19*, 503–511.

Pokhotelov, D., C. N. Mitchell, P. T. Jayachandran, J. W. MacDougall, and M. H. Denton (2009), Ionospheric response to the corotating interaction region-driven geomagnetic storm of October 2002, *J. Geophys. Res.*, *114*, A12311, doi:10.1029/2009JA014216.

Prölss, G. W. (1995), Ionospheric *F*-region storms, in *Handbook of Atmospheric Electrodynamics*, vol. 2, edited by H. Volland, pp. 195–248, CRC press, Boca Raton, Fla.

Rideout, W., and A. Coster (2006), Automated GPS processing for global total electron content data, *GPS Solut.*, *10*(3), 219–228, doi:10.1007/s10291-006-0029-5.

Ruohoniemi, J. M., and K. B. Baker (1998), Large-scale imaging of high-latitude convection with Super Dual Auroral Radar Network HF radar observations, *J. Geophys. Res.*, *103*, 20,797–20,811, doi:10.1029/98JA01288.

Shepherd, S. G., and J. M. Ruohoniemi (2000), Electrostatic potential patterns in the high-latitude ionosphere constrained by SuperDARN measurements, *J. Geophys. Res.*, *105*, 23,005–23,014, doi:10.1029/2000JA000171.

Sojka, J. J., R. W. Schunk, and W. J. Raitt (1981), Plasma density features associated with strong convection in the winter high-latitude *F* region, *J. Geophys. Res.*, *86*, 6908–6916, doi:10.1029/JA086iA08p06908.

Sojka, J. J., M. D. Bowline, and R. W. Schunk (1994), Patches in the polar ionosphere: UT and seasonal dependence, *J. Geophys. Res.*, *99*, 14,959–14,970, doi:10.1029/93JA03327.

Sojka, J. J., M. David, R. W. Schunk, and R. A. Heelis (2012), A modeling study of the longitudinal dependence of storm time midlatitude dayside total electron content enhancements, *J. Geophys. Res.*, *117*, A02315, doi:10.1029/2011JA017000.

Spiro, R. W., R. A. Heelis, and W. B. Hanson (1979), Rapid subauroral drifts observed by Atmospheric Explorer C, *Geophys. Res. Lett.*, *6*, 657–660, doi:10.1029/GL006i008p00657.

Thomas, E. G., J. B. H. Baker, J. M. Ruohoniemi, L. B. N. Clausen, A. J. Coster, J. C. Foster, and P. J. Erickson (2013), Direct observations of the role of convection electric field in the formation of a polar tongue of ionization from storm enhanced density, *J. Geophys. Res. Space Physics*, *118*, 1180–1189, doi:10.1002/jgra.50116.

Tsurutani, B., et al. (2004), Global dayside ionospheric uplift and enhancement associated with interplanetary electric fields, *J. Geophys. Res.*, *109*, A08302, doi:10.1029/2003JA010342.

Wang H., A. J. Ridley, H. Lühr, M. W. Liemohn, and S. Y. Ma (2008), Statistical study of the subauroral polarization streams: Its dependence on the cross polar cap potential and subauroral conductance, *J. Geophys. Res.*, *113*, A12311, doi:10.1029/2008JA013529.

Wang, H., H. Lühr, A. Ridley, and T. Huang (2014), The relative position of region 2 field-aligned current to subauroral polarization streams, *Ann. Geophys.*, *31*, 1521–1534.

Wang, W., J. Lei, A. G. Burns, S. C. Solomon, M. Wiltberger, J. Xu, Y. Zhang, L. Paxton, and A. Coster (2010), Ionospheric response to the initial phase of geomagnetic storms: Common features, *J. Geophys. Res.*, *115*, A07321, doi:10.1029/2009JA014461.

Wang, W., E. R. Talaat, A. G. Burns, B. Emery, S. Hsieh, J. Lei, and J. Xu (2012), Thermosphere and ionosphere response to subauroral polarization streams (SAPS): Model simulations, *J. Geophys. Res.*, *117*, A07301, doi:10.1029/2012JA017656.

Yizengaw, E., J. Dewar, J. MacNeil, M. B. Moldwin, D. Galvan, J. Sanny, D. Berube, and B. Sandel (2008), The occurrence of ionospheric signatures of plasmaspheric plumes over different longitudinal sectors, *J. Geophys. Res.*, *113*, A08318, doi:10.1029/2007JA012925.

Yuan, Z.-G., X.-H. Deng, and J.-F. Wang (2008), DMSP/GPS observations of intense ion upflow in the midnight polar ionosphere associated with the SED plume during a super geomagnetic storm, *Geophys. Res. Lett.*, *35*, L19110, doi:10.1029/2008GL035462.

Zou, S., A. J. Ridley, M. B. Moldwin, M. J. Nicolls, A. J. Coster, E. G. Thomas, and J. M. Ruohoniemi (2013), Multi-instrument observations of SED during 24–25 October 2011 storm: Implications for SED formation processes, *J. Geophys. Res. Space Physics*, *118*, 7798–7809, doi:10.1002/2013JA018860.